Journal of the Oceanographical Society of Japan
Vol. 47, pp. 249 to 264. 1991

The Steepness and Shape of Wind Waves*

Richard J. Bailey†, Ian. S.F. Jones‡ and Yoshiaki Toba¶

Abstract: Variations are found in the shape and the steepness of wind-generated surface gravity waves between very young waves, such as seen in a laboratory tank, and larger waves of various wave ages encountered at sea as the result of wind stress over larger fetches. These differences in the characteristic shape of wind waves are presented as a function of the wave age. The wave steepness is also expressed as a function of wave age, the measurement of which is consistent with the 3/2-power law connecting wave height and characteristic period, normalized by the air friction velocity.

1. Introduction

While much progress has been made by describing wind waves by considering the properties of their power spectral density in frequency, questions about the shape depend upon the description of "individual waves". Since wind driven waves have most of their spectral energy concentrated around a narrow range of frequencies, the record of water heights as a function of time can be analysed between zero crossings as a series of discrete waves. The earliest examples of this approach are the definitions of significant wave height and significant wave period. Considerable progress has been made, for example by Tokuda and Toba (1982), in determining the various statistical properties of individual waves.

In this paper we take the "individual wave" approach of Toba (1978), Tokuda and Toba (1981, 1982) and compare the wave shapes and the steepness of laboratory waves with ocean waves measured from a fixed platform. When the wind blows from the shore over the ocean, the waves generated become longer and less steep with distance offshore. If the wind is steady, a local equilibrium with the wind develops after a certain time. There are many situations where although the wind is flucuating and the site is far from shore, the wave spectrum is still in equilibrium with the wind over a range of frequencies. The peak frequency may be changing with time but the spectrum can be made universal by scaling it on this frequency and the wind stress. For such waves nearly in local equlibrium, a number of properties can be expressed in terms of the concept of wave age, the ratio of the phase speed of the waves to the wind friction velocity. Strict determination of the criteria for a wave field to be close to local equilibrium is left to the future, but the examples to be considered in this paper are the result of slowly changing wind and not too large wave age. Laboratory measurements of surface waves at short fetches, order 10 meters, are compared with open ocean waves which can have fetches of 10^6m.

Stokes (1847) showed that free waves should have sharper crests as they become steeper but the observation of such wave shapes is yet to be clearly documented on the ocean. When there is wind forcing, Cox and Munk (1954) showed over the ocean that the average slope of the lee side of waves was steeper than the average slope of the upwind

* Received 22 April 1991, in revised form 7 October 1991, accepted 9 October 1991.

† Marine Studies Centre, University of Sydney; present adress: CSIRO, Division of Oceanography, Hobart.

‡ Marine Studies Centre, University of Sydney.

¶ Department of Geophysics, Tohoku University, Sendai 980, Japan.

face of the wave implying that the wave was asymmetric. In the laboratory Plate (1978) examined the shape of waves and found sharp crests and non symetric shapes. More recently, Koga (1984) has had some success in relating the asymmetry of individual laboratory waves to their likeliness of breaking. Breaking waves were found to be more asymmetric in shape than non-breaking waves.

There are a number of advantages of treating each crest trough crest system as an "individual wave" and determining the individual waves statistical properties. Phenomena such as air flow separation depends upon the exact three dimensional form of the surface and such ideas have been recently reviewed by Csanady (1985). Power spectra, averaged over many ensembles, do not seem to provide the statistics needed.

2. Data collection

2.1. Bass Strait Data

The field data presented in this study were collected from ESSO/BHP's Kingfish B (KFB) and Barracouta (BCTA) oil-production platforms located in eastern Bass Strait. Bass Strait is a shallow coastal sea that connects the colder Southern Ocean with the Tasman Sea at a latitude of 40°S. Depth contours surrounding the platforms are shown in Fig. 1. Low pressure systems move east through Bass Strait, inducing large winds that frequently exceed 20 m s^{-1}.

Most of the field data were recorded using the KFB Data Acquisition System (Evans-Hamilton Model 4066) which is a microprocessor based system in which oceanographic and meteorological information is acquired and recorded at 0.5 second intervals on data cassettes.

A Baylor Wave Staff, which consists of two parallel 13 mm stainless steel wire ropes under tension at a spacing of 23 cm, was used to provide sea surface profile data. The wave staff is installed perpendicular to the water surface with one third to one half of the active length below mean water level. A tension of 15 kN is placed on the staff to maintain reasonable straightness of the wire ropes under extremes of wind and wave action. Sea water acts as a short circuit between the two wire ropes of the staff and the transducer injects an AC signal into the staff to sense the impedence. The Baylor Wave Staff is calibrated monthly by short-circuiting the staff at various points along its length using a specially designed

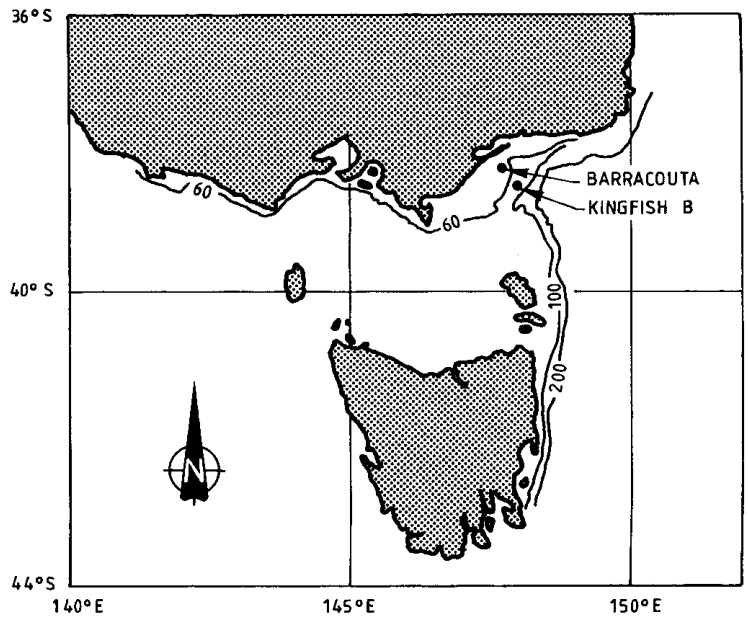

Fig. 1. Locations of the oil-production platforms in Bass Strait, showing the depths in meters.

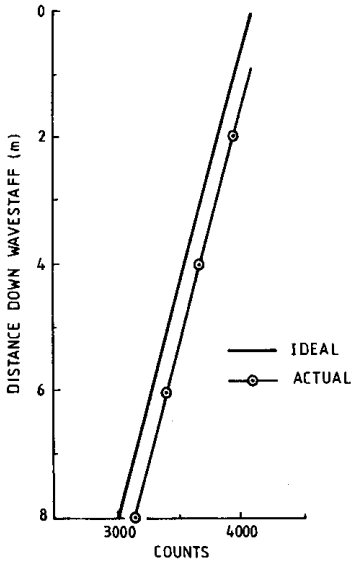

Fig. 2. Example of Bass Strait wavestaff calibration curve.

shortening bar to stimulate different constant water heights. An example of such a calibration is shown in Fig. 2. The offset of the readings, evident in this figure, does not affect wave height statistics. A Synchrotrac Wind Speed and Direction transmitter situated on a tower 65m (37m in one example) above mean sea level was used to provide wind speed and direction data.

To provide a control for the wave data recorded at the Kingfish B platform, wave data was also recorded from the Barracouta platform using a similar but simpler system to that described for the Kingfish B platform. Environmental data such as wind speed, wave period and significant wave height are recorded and averaged once per hour for a 1024 record period. A magnetic tape recorder was connected to the output voltage signal of the system, enabling a continual 4 Hz sampling of the wave profile when required.

2.2. *Laboratory Data*

The laboratory measurements were made in a wind-wave tunnel 0.6m wide, 1.2m high, and 20m long at the Physical Oceanography Laboratory, Tohoku University. Tank details are shown in Fig 3. The water depth was adjusted to be 0.6m and the wave reflections were reduced at the far end of the tank by a permeable mesh absorber.

Wave height was measured by enamel coated wires and a capacitance bridge. The frequency response, determined by a comparison with a gauge that was shaken to determine response, was about 10 Hz. Reference wind speeds were determined in the middle of the tunnel just near the air inlet to the water tank while the air friction velocity was determined from the wind speed profile.

Analogue FM tape recordings of the signals from the wind-wave tank allowed the surface elevation data to be processed on an OKITAC/50 digital computer. A sampling rate of 100 Hz was used.

3. Data Processing

Each data series was first transformed to remove the mean and any zero trend. From this time series, $\xi(t)$, the mean square elevation, $\overline{\xi^2}$, and the root mean square elevation,

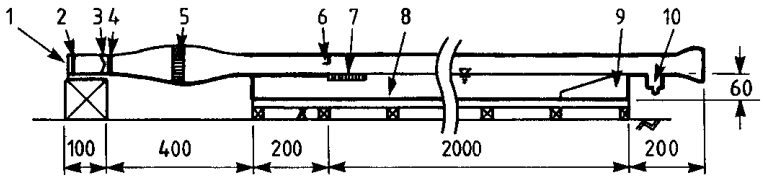

1. SHUTTER
2. AXIAL FLOW FAN
3. FLEXIBLE JOINT
4. FINE MESH SCREENS
5. HONEYCOMB
6. ANEMOMETER
7. JUNCTION PLATE
8. WATER TANK
9. WAVE ABSORBER
10. WATER OUTLET

Fig. 3. Schematic sketch of the wind-wave tunnel, Tohoku University. Dimensions shown are cm.

$\sqrt{\overline{\xi^2}}$, were calculated for the transformed surface elevations.

Power spectral density estimates for the transformed surface elevations were calculated using the technique proposed by Cooley and Tukey (1965) and a Hanning filter. The power spectral density, $\phi(f)$, is defined by

$$\overline{\xi^2} = \int_0^\infty \phi(f) df \qquad (1)$$

where f is frequency.

Throughout this study a zero-upcrossing definition is used for identifying individual waves in the transformed surface elevation data, $\xi(t)$. By this definition an individual wave is defined as the region between two consecutive up-crossings of the mean water level ($\xi = 0$) by the surface elevation profile, with a height H and period T, (see Fig. 4). Waves identified in this manner correspond fairly well to the standard conception of a wave consisting of a single crest and a single trough. Of course, only the dominant waves of the wave spectrum, and not the much smaller waves that may be riding on the surface of these dominant waves, will be identified by this procedure.

For each record the mean wave height ($\overline{H}$), the mean wave period ($\overline{T}$), along with the root mean square wave height (H_{rms}) are calculated. The significant wave height (H_S) is calculated as the average height of the highest one-thrid of the waves in the record. Two kinds of significant period are defined here: a) the mean period of the highest one-third of the waves (T_S) and b) the mean period of the longest one-third of the periods (T_S). The mean crest and trough amplitudes, a_c and a_t respectively, are also calculated including their 95% confidence limits about the means. Four measures of the wave profile symmetry are defined for each individual wave as the time from the up-crossing to the crest, T_1, the crest to the

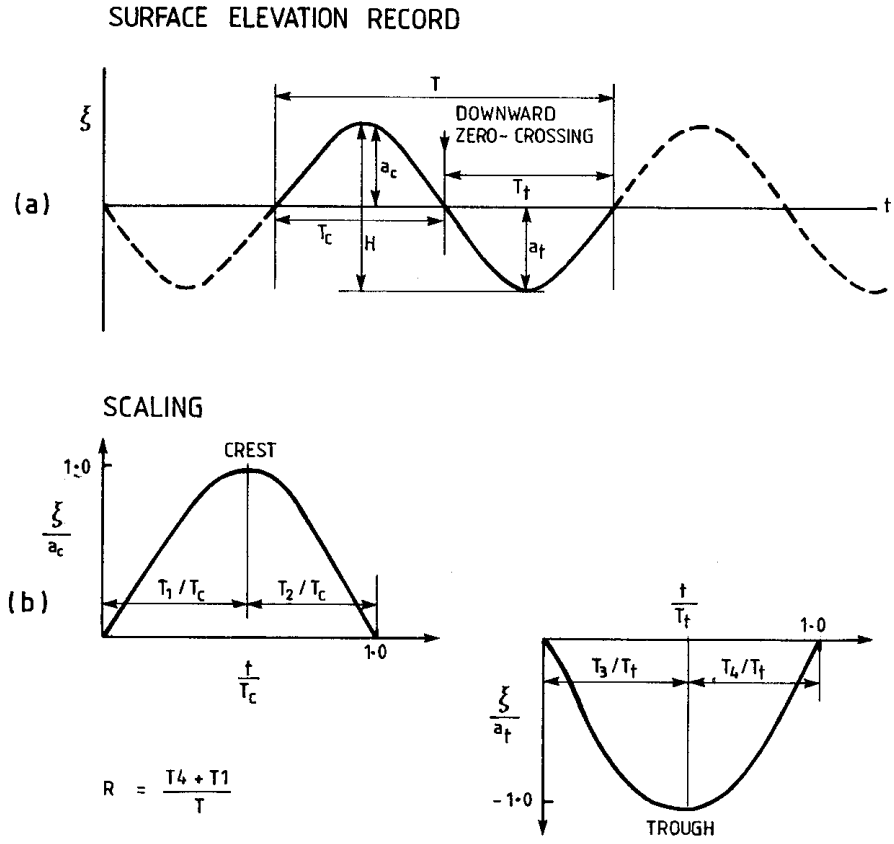

Fig. 4. Individual-wave nondimensionalising and averaging analysis.

down-crossing, T_2, and similarly for T_3 and T_4 as shown in Fig. 4. The overbar implies averages over many waves and in some cases the average of the normalized ratio, *e.g.* T_1/T_c.

3.1. The Non-dimensional Averaging Technique

As stated earlier, one of the main aims of this study is to detemine characteristic wind-wave profiles. This is achieved through the calculation of the nondimensional average wind-wave profile associated with each record studied.

The crest and trough profiles for each individual wave are scaled separately to have unit height and time span. The crest elevations are scaled by the crest amplitude (a_c), while the associated phase times, as measured from the beginning of the wave as defined by the first zero-upcrossing, are scaled by the time interval between the first zero-upcrossing and the zero downcrossing (T_c). The trough elevations are similarly scaled by the absolute value of the trough amplitude (a_t), and the time interval between the zero-downcrossing and the second zero-upcrossing (T_t).

This method of scaling the crests and troughs separately is chosen in preference to a total scaling of the wave by its height and period parameters, as this second method can create a distortion in the average wave profile if the positions of the zero-downcrossings for the constituent scaled individual wave profiles do not occur at a fixed distance between the two defining zero-upcrossings.

The scaled crest and trough profiles are next averaged separately to obtain characteristic nondimensional profiles for the given record (see Fig. 4). This averaging process finds the mean phase of the non-dimensional heights together with the 95% confidence limits. Averages performed in this manner are denoted by pointed brackets thus $\langle\ \rangle$. This method of averaging phase for a given height is chosen in preference to averaging elevations at given time as it eliminates distortions in the average wave-profile shape as a result of variations in the phase locations of the crest maxima and trough minima. For example, it can be shown that if two crest profiles, whose maxima lie at different phase locations, area averaged by this second procedure the resultant average profile is "flatter" in shape than either of the crest profiles that were used to form the average.

Table 1. General wave statistics.

Case	U_{ref} (ms^{-1})	u_* (ms^{-1})	Wave Age (c/u_*)	$\overline{H}$ (m)	H_S (m)	$\overline{T}$ (s)	T_S (s)	$T_{\S}$ (s)	C_S (ms^{-1})
WW1A	16.2	1.43	0.62	0.061	0.086	0.56	0.64	0.68	1.00
WW2A	11.5	0.57	1.11	0.031	0.045	0.41	0.45	0.48	0.70
YW1A	12.5	0.48	15.2	1.00	1.51	4.63	5.54	6.16	8.64
YW1B	16.6	0.67	10.4	1.16	1.81	4.46	5.23	6.15	8.16
YW2	16.9	0.68	12.6	1.60	2.53	5.45	6.58	7.54	10.26
BCTA	16.1	0.69	9.8	1.15	1.78	4.35	5.09	5.84	7.94
STORM24	19.7	0.92	13.3	3.22	5.21	7.80	10.15	11.17	15.83
STORM95	15.7	0.63	15.2	1.97	3.06	6.11	6.94	8.03	10.82
4HZ/KFB	14.0	0.71	14.2^+	2.40	3.81	6.45	8.45	9.26	13.32
CALM4HZ	5.0	0.20	33.0^+	0.81	1.29	4.36	5.34	5.86	8.33

U_{ref} is the reference wind speed at the entrance of the wind-wave tank for WW1A and WW2A, the wind speed at 65m level for the others, except at 37m level for STORM24.

$\overline{H}$: See Fig. 4.

T_S: Mean period of the highest one-third of the waves

$T_{\S}$: Mean period of the longest one-third of the waves

+ Calculated from estimated wind fields

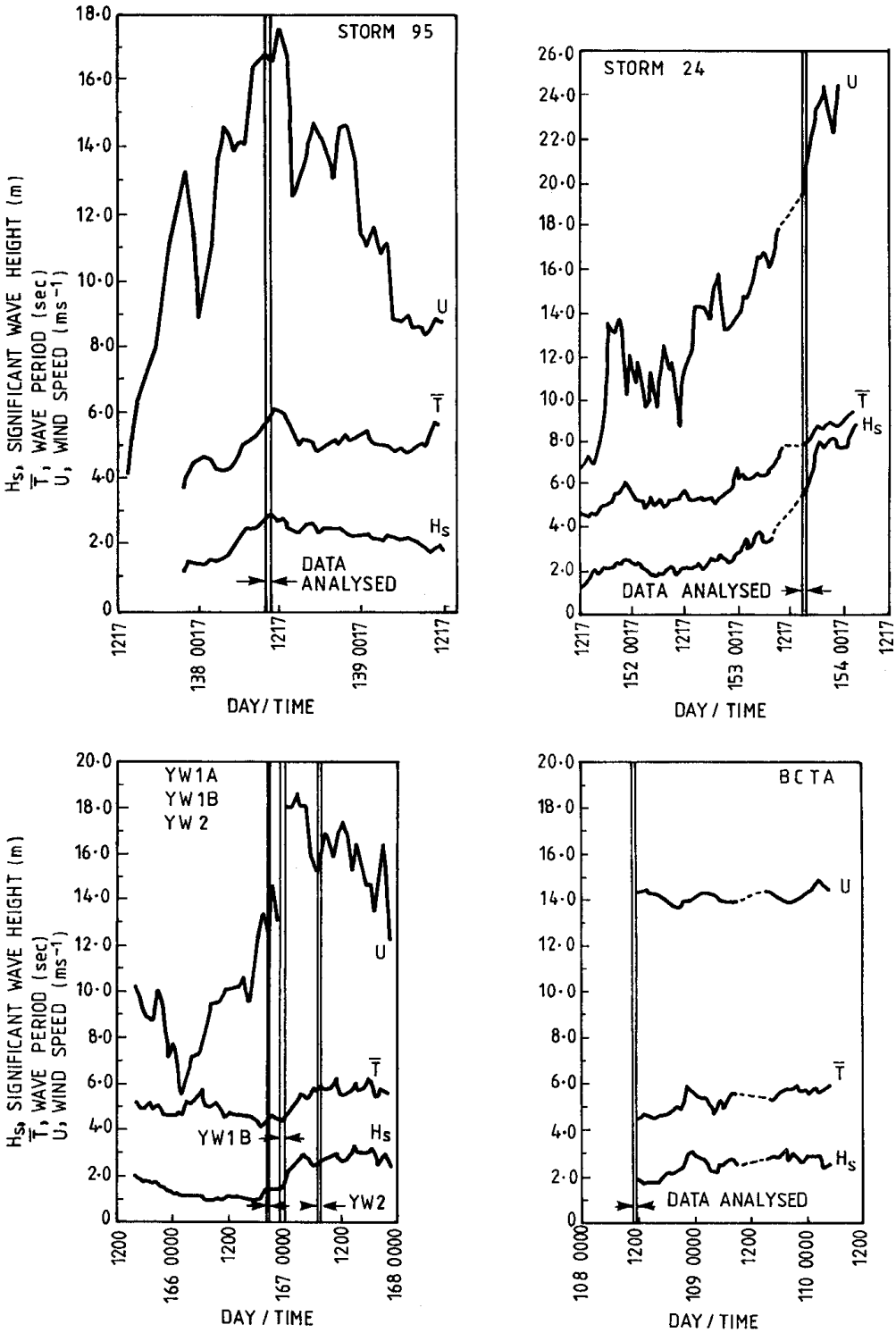

Fig. 5. Wind and wave history from data recorded in the NORMAL mode (17 min averages once per hour.)

In order to produce an averaged profile for the whole wave, the crest and trough averages are stretched and combined so as to produce a profile where the crest to trough magnitude $\bar{a}_c/\bar{a}_t$ and the crest to trough period $\overline{T}_c/\overline{T}_t$ were the same as the values for the individual waves. The total profile is finally rescaled to unit height by dividing the elevations by the crest to trough height of the newly reconstructed profile, and rescaled to unit period by dividing the phase times by the period of the reconstructed profile. This method of stretching and averaging has the disadvantage of not requiring the gradient of the profile at the zero crossings to be continuous but it has the advantage of producing a profile with the crest to trough ratio and the duration of the crest and trough in the same proportion as the average of the unscaled data.

4. Experimental results and discussion

4.1. Environmental Conditions

Ten different wind-wave cases were analysed, eight cases recorded in Bass Strait and two cases measured in the laboratory wind-wave facility. The general wave statistics of each case are given in Table 1. In this table the mean wave height ($\overline{H}$) and the significant wave height (H_S) along with the mean wave period ($\overline{T}$) and different measures for wave period are shown.

The ocean cases correspond to a range of conditions commonly observed at the two oil-production platforms in Bass Strait. This range includes recordings during the height of intense storms, the build up of such storms, and also during relatively calm conditions. In all cases the water is of sufficient depth that the waves are not considered to be affected by the sea floor.

Case STORM 95 was recorded during the peak of a storm (see Fig. 5) that occurred at the Kingfish B platform on 7 May 1980. The mean wind speed for the duration of this record was 15.7 m s^{-1}, measured at an elevation of 65 metres above mean sea level. Since it was blowing from the west it provided relatively fetch-limited conditions (see Fig. 1). The storm had been blowing for approximately 12 to 14 hr prior to the sampling time, and so the conditions for a fully developed sea, as given by Pierson *et al.* (1955), were not met.

Case STORM24 was similarly recorded at the Kingfish B platform, this time during the build up of a large storm that occurred on 2 June 1978 (see Fig. 5). The mean wind speed for the record was 19.7 m s^{-1}, measured (for this ocean case only) at 37 m above mean sea level. Again, the wind was blowing from the east providing unlimited fetch conditions. The storm had been blowing for approximately 24 hr prior to the sampling period, the conditions for a fully developed sea were also not met. However, Table 2 shows this case to have the largest significant wave height of the situations reported (5.21 m) even though the storm had yet to reach its peak.

The three cases YW1A, YWIB, and YW2,

Table 2 Wave shape parameters (CI: confidence level). See Fig. 4.

Case	$\bar{a}_c$(±95% CI) (m)	$\bar{a}_t$(±95% CI) (m)	$\bar{a}_c/\bar{a}_t$	$\overline{T}_c$(±95% CI) (s)	$\overline{T}_t$(±95% CI) (s)	$\overline{T}_c/\overline{T}_t$
WW1A	0.038±0.001	-0.024±0.001	-1.58	0.24±0.01	0.32±0.01	0.75
WW2A	0.018±0.001	-0.013±0.001	-1.38	0.19±0.01	0.23±0.01	0.83
YW1A	0.52±0.04	-0.48±0.04	-1.08	2.29±0.13	2.35±0.17	0.97
YW1B	0.60±0.03	-0.56±0.02	-1.07	2.19±0.07	2.27±0.07	0.96
YW2	0.83±0.04	-0.77±0.04	-1.08	2.65±0.10	2.80±0.11	0.95
BCTA	0.59±0.05	-0.56±0.04	-1.05	2.09±0.12	2.27±0.13	0.92
STORM24	1.64±0.09	-1.58±0.08	-1.04	3.91±0.16	3.89±0.14	1.01
STORM95	1.02±0.07	-0.95±0.06	-1.07	2.99±0.12	3.14±0.12	0.95
4HZ/KFB	1.23±0.10	-1.17±0.09	-1.05	3.20±0.20	3.25±0.19	0.98
CALM4HZ	0.41±0.04	-0.40±0.04	-1.03	2.17±0.14	2.20±0.15	0.99

were recorded at different stages of one particular storm that occurred at the Kingfish B platform on 15 and 16 June, 1985. The mean wind speed for YW1A was 12.5 m s^{-1}, blowing from the north-west. Only 8 min of data were available to be analysed. Case YW1B corresponds to the build up of the storm, with the mean wind speed for the record now having increased to 16.6 m s^{-1} from the west. The last case in the set, YW2, corresponds to the storm after it reached its peak.

Case BCTA was recorded at the Barracouta platform on 18 April 1985 (see Fig. 5). The mean wind speed during the recording was 16.1 m s^{-1}, yet again blowing from the west. These conditions provide for shorter fetch-limited conditions than can occur on the Kingfish B platform due to the closer proximity of the Barracouta platform to the coast (see Fig. 1).

The two cases CALM4HZ and 4HZ/KFB were both recorded at the Kingfish B platform at a 4Hz sampling rate in a similar manner to case BCTA. Unfortunately, during these two cases the KFB Data Acquisition System did not successfully log the accompanying meteorological data, and so the platform's regular weather reports were used to estimate the conditions. From such reports it is concluded that case CALM4HZ was recorded during calm ocean conditions on 20 June 1984, the mean wind speed being approximately 5 m s^{-1} from the north north-west. This case, therefore, corresponds to conditions of very little wind forcing. The calm conditions are also evident in the low mean wave height and significant wave height as seen in Table 1. Case 4HZ/KFB, on the other hand, was recorded during a storm that occurred on 22 June, 1984. The mean wind speed for this recording was approximately 14 m s^{-1} from the west. A large significant wave height, 3.81 m, was observed (see Table 1).

4.2. *Wave Age - The wind/wave coupling parameter*

The wave age, defined here as the ratio of the phase speed of the average individual-wave (*i.e.* the conventional linear wave phase speed relative to the underlying water), c, to the wind frictional velocity, u_*, is given for each case in Table 1. The individual-wave phase speed for a free gravity wave is estimated from the mean wave period, $\bar{T}$, according to

$$c = \frac{g\bar{T}}{2\pi} \tag{2}$$

When the significant period is defined as the average period of the highest one-third of the waves, T_S, the phase speed is given by

$$C_S = \frac{gT_S}{2\pi} \tag{3}$$

The wind friction velocity, u_*, for the ocean cases is calculated in a way similar to Toba *et al.* (1990), but using the overall roughness length, z_0, of their expression eq. (30), *i. e.*

$$\frac{g\,z_0}{u_*^2} = 0.020\left(\frac{g}{\sigma_p\,u_*}\right)^{\frac{1}{2}} \tag{4}$$

This expression, which produces a drag coefficient that is dependent on the properties of the sea surface, characterised by the peak spectral frequency $\sigma_p = 2\,\pi\,/\,1.05\,T_S$ is most easily used by consulting their Fig. 17. A logarithmic wind profile is assumed since the air-sea temperature difference was small according to some data cited by Toba *et al.* (1990) and used for calculating U_{10} from the recorded wind speed which was measured, for all but one case, at 65 metres above mean sea level. The wind frictional velocity for the laboratory cases was estimated directly from measurements of the wind velocity profile.

If one considers the relative forcing of the wind on the dominant waves to be dependent on the ratio of the wave phase speed to the wind frictional velocity, then as Table 1 shows, the laboratory wind-waves were the most strongly forced waves analysed in this study. The laboratory wind-waves were the "youngest" waves, *i.e.* the wind frictional velocities were of the order of, or greater than, the average linear wave phase speeds of the waves. In contrast, the dominant ocean wind-waves recorded in Bass Strait were much "older" than the laboratory wind-waves. The average phase speeds of these waves were approximately one order larger than the wind frictional velocities, with the ratio, C_S/u_* varying from 12 to 42 (*c.f.* Table 1). The wave age for case YW1B is observed to be accordingly lower than the wave age for case YW1A due to the increase in wind speed with the onset of the storm. As the wave field developed and grew under the in-

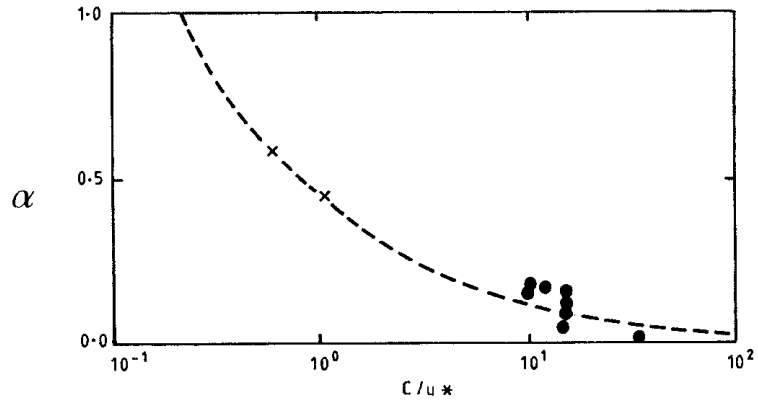

Fig. 6. Skewness coefficient α of the surface elevation probability distributions as a function of wave age c/u_*. (The dashed curve is an approximate fit to the data.) Filled points are field data. Crosses represent laboratory data.

fluence of the storm, however, the wave age decreased again; this is observed for the wave age of case YW2.

4.3. Nonlinearity and surface elevation

The power spectral densities for each of the events are not shown, but all spectra show single dominant peak frequencies in the wind-generated frequency band, with no dominant frequencies at shorter, or swell frequencies, being observed. All spectra, except for case CALM4HZ, do show secondary minor peaks at approximately twice the dominant frequency, indicating that a certain degree of energy is associated with the second harmonics for these cases. This was particularly observed in the spectra for the laboratory cases, WW1A and WW2A.

The dependence on wave age (c/u_*) of the skewness of the normalised surface elevation probability distributions, as given by the skewness coefficient, α, where

$$\alpha=\frac{1}{\xi_{\mathrm{rms}}^3}\cdot\frac{1}{N}\sum_{i=1}^{N}(\xi_i-\bar{\xi})^3 \qquad (5)$$

is shown in Fig. 6. The greatest skewness, and hence deviation from the Gaussian, occurs for the youngest wave case, WW1A. The positive skewness of the distributions suggest that the surface profiles are characteried by waves with sharper crests and shallower troughs than would be found for free waves obeying linear equations, indicating the presence of bound harmonics. The energies associated with the second harmonics of cases WW1A and WW2A were particularly evident in the spectra for these cases. Similar deviations from a Gaussian probability distribution of heights were also found in the laboratory observations of Huang and Long (1980) and Plate (1978). The oldest wave case, CALM4HZ, has almost a zero value for the skewness coefficient as would a Gaussian distribution. It may be recalled that case CALM 4 HZ was recorded during calm conditions where the wave field was dominated by swell rather than by wind forcing, and thus where the linear model of free sinusoidal components is generally assumed to be adequate.

Very significant differences at the 95% confidence level are shown in Table 2 between the average crest amplitudes, $\bar{a}_c$, and the average trough amplitudes $\bar{a}_t$, for the two laboratory cases. For case WW1A the average crest amplitude is 58% greater than the average trough amplitude, and 38% greater for case WW2A. For the ocean cases, the crests are still constantly higher than the troughs, although these differences are not statistically significant. The average crest excursion times, $\bar{T}_c$, for the laboratory wind-waves are correspondingly shorter than the average trough excursion times, $\bar{T}_t$, whereas very little difference is observed between the average crest and trough excursion times for the ocean wind-waves. This supports the sharp crest and shallow trough view of waves for the laboratory cases.

4.4. Wave Steepness

The deviations from a sinusoid shape encountered so far conceivably arise because the free sinusoidal components of the linear model only satisfy the first-order equations of motion, and therefore only hold true when the wave steepness, ak, approaches zero. For real wave fields, such as observed here, the wave steepness is finite. For such cases a more accurate description of the surface profile requires contributions from higher-order approximations, such as given by Stokes (1847), where

$$\xi(x, t)=a\sin x+\frac{a^2k}{2}\sin 2x+\frac{3a^3k^2}{8}\sin 3x+\cdots \tag{6}$$

and where the phase

$$x=(kx-\sigma t+\delta) \tag{7}$$

is expressed in terms of the wavenumber k, the radian frequency σ, and a constant phase δ. The resulting profile from Eq. (6) will show increasingly sharper crests and shallower troughs with higher values of ak as a result of the increasing distortion of the surface profile by the harmonic components. The profile will no longer be symmetric with respect to the mean water level, and the surface elevation distribution will not be Gaussian.

Hsu *et al.* (1982) found wave steepness, as measured from spectral properties, to depend upon the wave age, c/u_* (where c was determined from the dominant wave frequency). In terms of individual waves we can use the significant wave height and the zero crossing periods to calculate a wave steepness. If one assumes the self similarity relation first advanced by Toba (1972) for significant wave height and period, *i.e.*

$$H_S=B\,(gu_*)^{1/2}T_S^{3/2} \tag{8}$$

one can reform this to be an expression in terms of height and wavenumber. We note that the period, observed fixed to the earth, and the wave length, are related by a velocity that includes any convection of the waves by the underlying fluid u. Thus

$$T=\frac{2\pi}{k(c+u)} \tag{9}$$

or for "significant"quantities

$$T_S=\frac{2\pi}{k_SC_S\left(1+\dfrac{u}{u_*}\dfrac{u_*}{C_S}\right)} \tag{10}$$

For large phase speeds u is small compared with C_S and can be neglected, but for laboratory results this is not the case. Tokuda and Toba (1982) suggest for laboratry waves

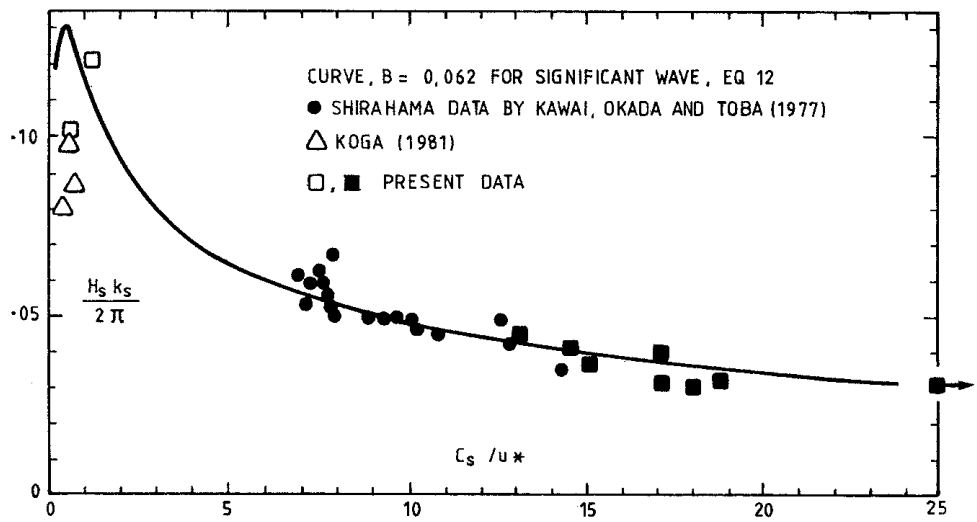

Fig. 7. Significant wave slope as a function of wave age. Notice C_S is the phase velocity of the significant wave calculated from the wave period observed in a fixed frame of reference. The filled points are field data.

$$\frac{u}{u_*}=0.206 \tag{11}$$

where u is an "effective drift velocity" that takes into account "bound wave effects" and other processes involved in the transfer of momentum from the wind to the water. Substitution of Eq. (11) into Eq. (10) and manipulation of Eq. (8) in a slightly different manner of Tokuda and Toba (1982) produces an expression for the significant slope

$$\frac{H_S k_S}{2\pi}=(2\pi)^{1/2}B\left(\frac{C_S}{u_*}\right)^{\frac{1}{2}}\left\{1+0.206\left(\frac{C_S}{u_*}\right)^{-1}\right\}^{\frac{2}{3}} \tag{12}$$

where B is an empirical constant. The above expression is for a steepness calculated from the significant wave height and wave number and is a more appropriate use of the term "significant steepness" than that, say, used by Huang et al. (1981). Note that while Eq. (12)

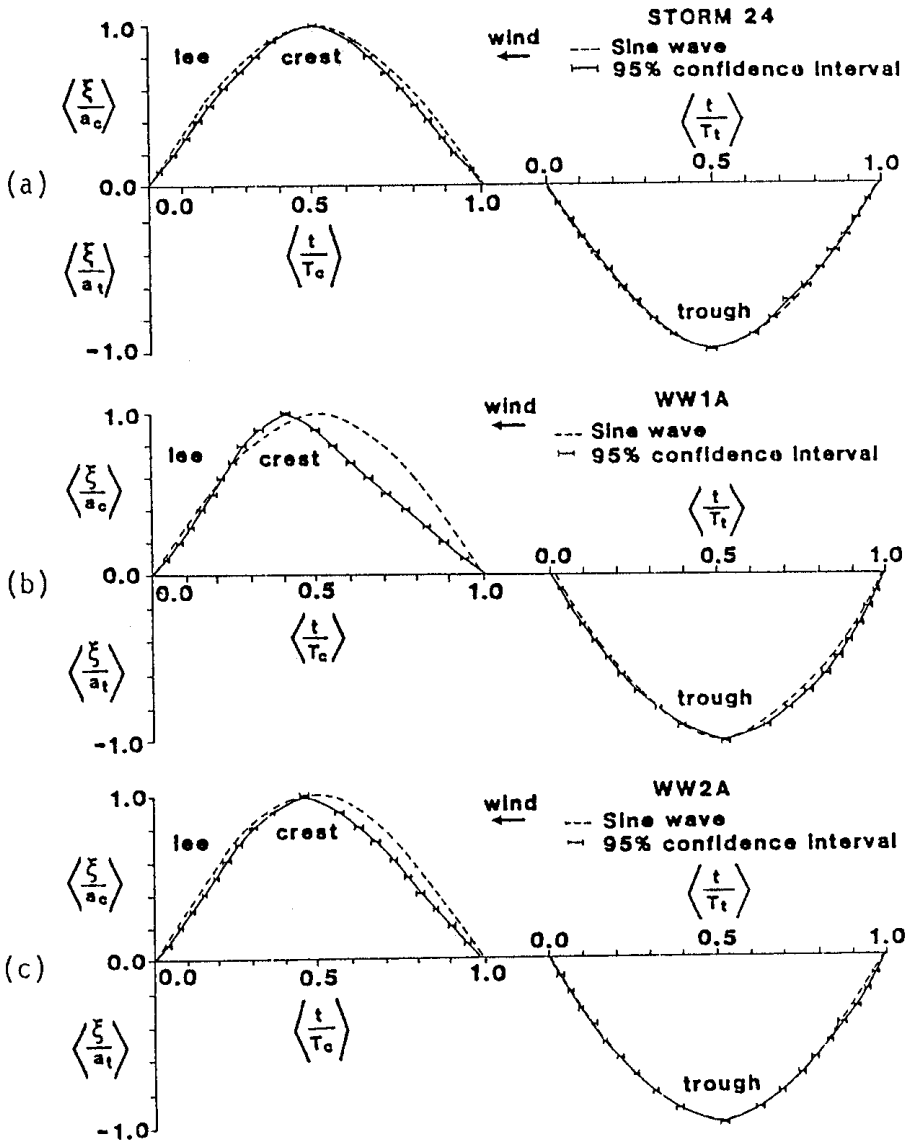

Fig. 8. Average nondimensional crest and trough profiles for three difference cases: (a) an ocean case, STORM24; (b) a laboratory case, WW1A; (c) a laboratory case, WW2A.

is different to the expression shown in Toba (1988) it is but an alternative.

In Figure 7 we have plotted the significant slope results from the present study together with the Shirahama data of Kawai *et al.* (1977) and results collected in the present tank by Koga (1981). Both Eq. (12) and the measurements show increased significant wave slope for younger waves, but Eq. (12) predicts that the youngest waves have a significant wave slope less than the maximun value, 2.1 B, of $H_S k_S / 2\pi$. The predicted steepness in this region is dominated by the phase speed correction employed in Eq. (11). At these very low values of c/u_* the expression of Eq. (12) overpredicts the significant wave steepness for the experiments, possibly because the significant wave number, k_S, is deduced from the square of the significant wave period rather than directly measured. The rather clear dependence of significant slope on wave age in Fig. 7 relies on the wave field being dominated by local wind forcing. When u_* is no longer an important variable, as for example for swell, we cannot expect wave age to be the dominant determinant of slope. The three-half power law of Eq. (8) is only realised for wave fields that are in "local equilibrium" with the wind and so the same restriction would apply to the expression for slope, Eq (12).

4.5. *Asymmetry and Symmetry Characteristics of Wind-Wave Profiles*

Figure 8(a) shows the results from the separate crest and trough analysis for the ocean case, STORM24. The crest and trough profiles for this case were, in general characteristic of the other ocean cases. A sinusoidal wave representing the linear free wave model is provided for comparison. The wind is blowing in the same direction as the dominant wave forms are travelling, *i.e.* from right to left. At the 95% confidence level, the average crest profile is slightly more peaked than the corresponding sinusoidal wave, but similarly symmetric. The trough profile is well approximated by the sinusoidal model.

Significant deviation from the sinusoidal model is found for the laboratory cases (Figs. 8 (b) and (c)). Asymmetry is observed for the crest profiles, particularly for the youngest case WW1A, where the leeward face is much steeper than the windward face. The average crest profiles for the laboratory cases are therefore found to lean over with the wind. Very little asymmetry is observed for the

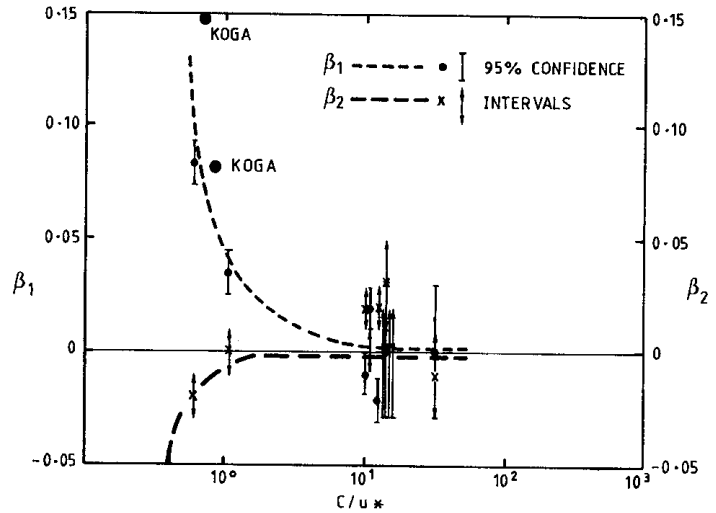

Fig. 9. The degree of asymmetry of the average nondimensional crest profiles $\{\beta_1 = 0.5 - (\overline{T_1 / T_c})\}$ and trough profiles $\{\beta_2 = 0.5 - (\overline{T_3 / T_t})\}$ as a function of waves age c/u_*. For symmetric waves both β_1 and β_2 are zero. (T_1 / T_c) and (T_3 / T_t) are the averaged scaled phase locations of the crest maxima and trough minima, respectively. (The dashed curves are approximate fits to the data.)

Table 3. Wave asymmetry parameters

Case	$\overline{T_1}$ (s)	$\overline{T_2}$ (s)	$\overline{T_3}$ (s)	$\overline{T_4}$ (s)	R
WW1A	0.10	0.14	0.17	0.15	0.45
WW2A	0.09	0.10	0.11	0.11	0.49
YW1A	1.15	1.14	1.16	1.19	0.51
YW1B	1.11	1.08	1.10	1.17	0.51
YW2	1.37	1.28	1.36	1.45	0.52
BCTA	1.02	1.07	1.11	1.15	0.50
STORM24	2.02	1.90	1.91	1.98	0.51
STORM95	1.55	1.43	1.54	1.60	0.52
4HZ/KFB	1.62	1.58	1.52	1.74	0.52
CALM4HZ	1.08	1.09	1.15	1.05	0.49

See Fig. 4 for an explanation of the symbols.

trough profiles. This seems plausible as the influence that the wind forcing has on a wave profile is presumably concentrated in the crest region. This is the part of the profile that extends most into the wind field. It may also be recalled that asymmetry was inferred from glitter photographs of the ocean by Cox and Munk (1954) from the downwind shift in the peak of the downwind wave-slope distribution for waves.

The asymmetry in the wind-wave crest profiles, and to a lesser extent the trough profiles, is shown in Fig. 9 to be dependent on wave age (as was wave steepness). The degree of asymmetry is given by the deviation of the scaled values for T_1 and T_3 from a symmetric value of 0.5 (β_1 and β_2 respectively-see Fig. 4). Numerical values are available in Table 3.

Where the relative forcing of the wind on the dominant wave profile is considered greatest, *i.e.* for young wave age, the greatest asymmetry is observed. At the 95% confidence level shown, only a small deviation from the symmetric value of 0.5 is observed for the ocean cases, whereas significant deviation is observed for the laboratory cases, especially for the crest profile.

A very similar statistic can be extracted from Koga (1984). While he defined his waves about the crossing of the mid point of the crest and trough, his statistic for t_3/t_1 is similar to our T_1/T_c, and t_4/t_2 is similar to our T_2/T_c in

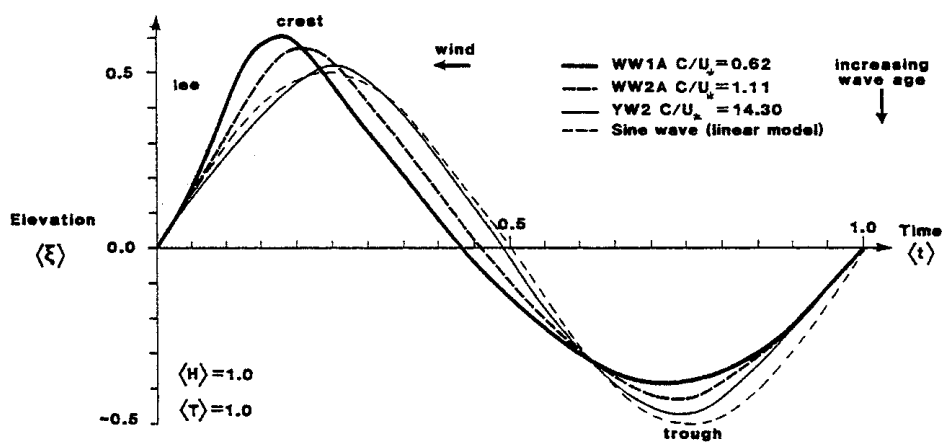

Fig. 10. Comparison of characteristic nondimensional wind-wave profiles of different wave age c/u_*.

the present analysis. Fig. 9 shows Koga's two points.

In general, these results complicate any application of a linear free wave model description to the younger wind-wave cases. As the younger waves are asymmetric on the average in time, this implies that the wind-wave profiles must be characterized by bound harmonics to describe this asymmetry. The use of the linear model will fail as the free components will disperse at different phase speeds depending on the frequencies, and hence an asymmetric profile shape cannot be maintained in time. Similarly, asymmetry of wind-wave profiles cannot be ascertained from a power spectral decomposition of a wind-wave field, as any information on the phase relationship between the wave components is lost in the process.

4.6 Combined Characteristics of the Wind-Wave Profiles

The average nondimensional wind-wave profiles that result from the combination of crest and trough profiles in the proportions of the unscaled individual waves are given in Fig. 10. These results now draw together the findings on the characteristic profile and upwind-downwind asymmetries of the observed wave fields. Case YW2 is shown as a typical ocean case. Since the average profile is computed from a time series, it can be thought of as a one-dimensional cut in the direction of propagation of the characteristic wave. The three-dimensionality of wave fields can not be addressed from the present class of data.

The laboratory wind-waves are characterized by asymmetric profiles with sharp crests and shallow troughs, the leeward face being steeper than the windward face. The average nondimensional wave shapes of Plate (1978) also show somewhat the same character as found for the laboratory cases here. On closer inspection a certain degree of asymmetry (in the horizontal plane) is also shown for the stronger wind case ($u_\infty = 15$ m s^{-1}) of Plate, although he did not draw attention to it.

The dominant ocean wind-waves, in contrast, are characterized by approximately sinusoidal and symmetric profiles. Although not shown, this was particularly evident for case CALM4HZ, which was recorded during conditions where little asymmetry was expected. A small degree of asymmetry was observed for case BCTA which is one of the youngest wave-age cases observed in the ocean, and which is also the case corresponding to the most fetch-limited conditions of the ocean cases. Very little change was observed in the characteristic wave profile shape for the three cases YW1A, YW1B, and YW2, which correspond, as may be recalled, to a sequence of recordings during one particular storm at the Kingfish B platform.

The coupled dependence of both the nonli-

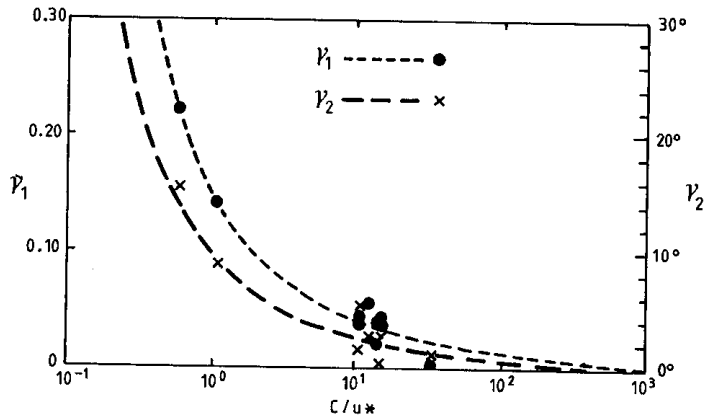

Fig. 11. The relationship to wave age c/u_* of the nonlinearity of the characteristic nondimensional wind-wave profiles as measured by the ratio of the magnitude of the second harmonic to the magnitude of the fundamental (γ_1), and of the asymmetry as measured by the phase difference of the fundamental from 90° (γ_2). (The dashed curves are approximate fits to the data.)

nearity and asymmetry of the wind-wave profiles on wage age, c/u_*, is shown in Fig. 10. The two laboratory cases are shown together with case YW2 as a typical ocean case, and also a sinusoidal wave representing the linear model. Quantitatively, this dependence on wave age is shown for all the cases in Fig. 11. The nonlinearity of the dominant waves is measured by the ratio of the magnitude of the second harmonic to the magnitude of the fundamental (γ_1), as calculated by standard Fourier analysis, and the asymmetry is measured by the phase difference of the consine fundamental from 90 degrees (γ_2). For a linear and symmetric wave both γ_1 and γ_2 are equal to zero. This is very close to being observed for case CALM4HZ.

5. Conclusions

As the importance of wind forcing on wind waves changes, so do many properties of the waves. A reasonable measure of this wind forcing is wave age, defined as c/u_* where c is defined as the linear wave phase speed for the "dominant wave" present. We have shown that an average profile of the "individual waves" that go to make up the rough sea surface can be determined, and that the form of this average profile is a function of the wave age. An average profile defined between zero crossings only exists because the spectrum of the ocean surface height is narrow and peaked around a characteristic frequency. While the technique of scaling each portion of height profile between zero crossings extends the technique to a finite band width process, high frequency averaging is inherent in the technique.

Although no waves of intermediate wave age were analysed for wave shapes in this study, it is proposed from the results obtained suggest that nonlinear and asymmetric dominant-wave profiles of young wave age evolve, under the action of the wind, into more linear and symmetric free waves at older wave ages. The ocean in general is far more complicated than the wind-wave tank due to the occurrence of a wide range of random and variable forcing conditions.

The characteristics of the shorter waves will be further modulated by the dynamics of the underlying dominant wave motion. If so, this may well explain the skewness in the slope distribution observed by Cox and Munk (1954) for their ocean data in contrast to the symmetric characteristics of the dominant ocean wind-waves observed in this study. The asymmetry in the slope distribution for the Cox and Munk data may arise due to a significant contribution to the skewness from the shorter-scale waves rather than from the asymmetry of the characteristic wave. Here we have described only the shape of dominant wave. But such knowledge may prove useful in the understanding of shorter wave phenomena such as influence of microwave backscattering used for remote sensing purposes. One expects air flow separation to depend upon the wave profile and so the marked change of asymmetry of the wave as c/u_* varies suggests that the separation seen over young laboratory waves may be less frequent over the older ocean waves. Wave breaking has also been shown to depend in part on the shape of the wave profile and these measures decrease with wave age.

Other measures of the wave field such as skewness of the probability distribution of the surface are also shown to decrease with wave age. Finally it has been known for some time that the maximum slope of the characteristic wave, depicted by $H_S k_S$, decreases as the waves mature. Altogether we have a picture of a transition of wave properties from steep asymmetric waves with strong air flow separation to passive swell.

Acknowledgements

We wish to thank ESSO-BHP for allowing us to make measurements over a number of years from their Bass Strait Platforms. Dr Hiroshi Kawamura kindly collaborated on the laboratory experiments. This study was partially supported by a grant under a Monbusho International Scientific Research Program.

References

Cooley, J.W. and J.W. Tukey (1965): An algorithm for the machine calculation of complex Fourier Series, Math. Comp., **19**, 297-301.

Cox, C. and W. Munk (1954): Statistics of the sea surface derived from sun glitter. J. Mar. Res., **13**, 198-227.

Csanady, G.T. (1985): Air-sea momentum transfer by means of short-crestd wavelets. J. Phys. Oceanogr., **15**, 1486-1501.

Huang, N.E. and S.R. Long (1980): An experimental study of the surface elevation probability distribution and statistics of wind-generated waves. J.Fluid Mech., **101**, 179-200.

Huang N.E., S.R. Long, C.Tung, Y.Yuen and L.F. Bliven (1981): A unified two-parameter wave spectral model for a general sea state. J.Fluid Mech., **112**, 203-224.

Hsu, C., H. Wu, E. Hsu and R.L. Street (1982): Momentum and energy transfer in wind generation of waves. J. Phys. Oceanogr., **12**, 929-951.

Kawai, S., K.Okada and Y.Toba (1977): Field data support of three-seconds power law and $gu_*\sigma^{-4}$-spectral form for growing wind waves. J. Oceanogr. Soc. Japan, **33**, 137-150.

Koga, M. (1981): Direct production of droplets from breaking wind-waves: its observation by a multi-colored overlapping exposure photographing technique. Tellus, **33**, 552-563.

Koga, M. (1984): Characteristics of a breaking wind-wave field in the light of the individual wind-wave concept. J. Oceanogr. Soc. Japan, **40**, 105-114.

Pierson, W.J., G. Neumann and R.W. James (1955): Practical methods for observing and forecasting ocean waves by means of wave spectra and statistics. U.S. Dept. of the Navy Hydrog. Offc. Publ. No. 603, 284 pp.

Plate, E. J. (1978): Wind-generated water surface waves: The laboratory evidence. In "Turbulent Fluxes through the sea surface, Wave Dynamics, and Prediction", Edited by A. Favre and K.Hasselmann, Plenum Press, New York, 385-401.

Stokes, G.G. (1847): On the theory of oscillatory waves. Trans. Camb. Phil. Soc., **8**, 441-455.

Toba, Y. (1972): Local balance in the air-sea boundary processes, I. On the growth process of wind waves. J. Oceanogr. Soc. Japan, **28**, 109-120.

Toba, Y. (1978): Stochatic form of the growth of wind waves in a single-parameter representation with physical implications. J. Phys. Oceanogr., **8**, 494-507.

Toba, Y. (1988): Similarity laws of the wind wave and the coupling process of the air and water turbulent boundary layers. Fluid Dyn. Res., **2**, 263-279.

Toba, Y., N. Iida, H. Kawamura, N. Ebuchi and I.S.F. Jones (1990): Wave dependence on sea-surface wind stress. J. Phys. Oceanogr., **20**, 705-721.

Tokuda, M. and Y. Toba (1981): Statistical characteristics of individual waves in laboratory wind waves. I. Individual wave spectra and similarity structure. J. Oceanogr. Soc. Japan, **37**, 243-258.

Tokuda, M. and Y. Toba (1982): Statistical characteristics of individual waves in laboratory wind waves. II. Self-consistent similarity regime. J. Oceanogr. Soc. Japan, **38**, 8-14.

風波の波形勾配と形状について

R.J. Bailey*,†, I. S. F. Jones*, 鳥羽良明¶

要旨： 風で起きる表面重力波の形状と波形勾配に，実験室でみられるような非常に若い波と，長い吹走距離にわたる風の応力の結果として現れる，いろいろな波齢の，より大きい波との間に，変化が見いだされた．風波の特徴的な形状におけるこれらの違いを，波齢の関数として提出した．波形勾配も波齢の関数として表現されるが，その測定値は，空気の摩擦速度で規格化した波高と特性周期を結び付ける3／2乗則と両立するものである．

*オーストラリア　シドニー大学海洋研究センター
† 現所属：ホバート市　CSIRO 海洋部
¶ 東北大学理学部
〒980　仙台市青葉区